

# Monitoring Local Shoreline Changes by Integrating UASs, Airborne LiDAR, Historical Images and Orthophotos

Gil Gonçalves<sup>1,2</sup>, Sara Santos<sup>1</sup>, Diogo Duarte<sup>3</sup> and José Gomes<sup>1,4</sup>

<sup>1</sup>University of Coimbra, Portugal

<sup>2</sup>Institute for Systems Engineering and Computers at Coimbra, Portugal

<sup>3</sup>Faculty of Geo-Information Science and Earth Observation (ITC), The Netherlands

<sup>4</sup>Centre of Studies on Geography and Spatial Planning, Portugal

**Keywords:** Coastline Erosion, Local Change Rate, Drones, DSM, DSAS, GIS.

**Abstract:** Shorelines are continuously changing in shape and position due to both natural and anthropogenic causes. The present paper is a two-fold goal: 1) analyse the relevance of low-cost UAS (Unmanned Aerial Systems) imagery for local shoreline monitoring and control of topo-morphological changes by using the derived Digital Surface Models (DSM) and orthophotos; 2) integrating this 2.5D and 2D geospatial data with airborne LiDAR, historical images and national orthophotos series to assess the Furadouro's beach erosion and shoreline change between 1958 to 2015. Digital Surface Models (DSM) derived from airborne LiDAR and low cost UAS are used to delineate the shoreline position for the years 2011 and 2015. A time series of shoreline positions is then obtained by combining the shoreline obtained from the DSM and LiDAR data with historical shoreline positions recovered from aerial images and orthophotos for the years 1958, 1998 and 2010. The accretion and erosion rates, generated by using the Digital Shoreline Analysis System (DSAS), shows that the integration of the several Geospatial technologies was very effective for monitoring the shoreline changes occurred in this 57-year interval, revealing an average shoreline retreat of -2.7 m/year. In addition, the DSMs derived from UAS technology can also be effectively used in the topographic monitoring of the primary dunes or in other processes associated with the coastline erosion phenomena.

## 1 INTRODUCTION

Over the years, population growth in coastal areas has been increasing, concentrating in such locations economic, political and social centres. This growth was very swift and poorly planned, creating urban and industrial pressures. Consequently, we've had several coastal environments destroyed, which have caused the increase in territorial vulnerability to coastal erosion processes.

In this extremely dynamic context, the shoreline continuously changes its position and shape through time. To map the temporal evolution of the shoreline it is necessary to consider a spatial feature (or a shoreline proxy) that is coherent in space and time in order to reduce the positional uncertainty (Cenci et al., 2017). The literature concerning this issues reveals the existence of several shoreline proxies (e.g. mean low of water line, base/top of bluff/cliff, vegetation line, etc.) and mapped using multi-temporal geospatial data sources, such as satellite

imagery, historical air photos, orthophotos series, LiDAR data, GPS profiles, etc. (Albuquerque et al., 2013; Cenci et al., 2017; Moore, 2000; Sousa et al., 2018).

Different geospatial technologies have also been used to monitor foredunes and shoreline changes at a local scale. Among these technologies we can refer: i) the use of Airborne LiDAR combined with aerial imagery and Global Navigation Satellite Systems (GNSS) data for the quantification of the deflation and horizontal migration of a group of active dunes in the United States (Hardin et al., 2014); ii) the use of Network Real Time Kinematics (NRTK) positioning technologies, supported by active regional GNSS networks to monitor at a local scale the morphology changes of a group of dunes due to erosion and accretion (Garrido et al., 2013); iii) the comparison of UAS aerial imagery and its derived 3D models through dense image matching with terrestrial laser scanner (Gonçalves et al., 2018; Mancini et al., 2013). In both cases, 3D data used in this approach has a

vertical accuracy of 0.19 m for the Root Mean Square Error (RMSE); iv) the use of UAV images to generate a 3D model and determine the morphological changes with a resolution of 10cm and vertical RMSE of 5 cm (Gonçalves and Henriques, 2015).

As above mentioned, one of the main purposes of the present paper is to integrate DSM data and orthophotos, both derived from UAS Photogrammetry, with existing geospatial data (2D and 2.5D) for monitoring local shoreline changes. The next section presents some of the main features concerning the study area. This is followed by the description of the various types of Geospatial technologies used in this work. Details of the accuracy of the UAS images, shoreline change methods, the results obtained and its discussion are thus presented in a subsequent section. Finally, a brief synopsis and final conclusions of the paper are presented.

## 2 STUDY AREA

Furadouro's beach is located in the northern part of Portugal (Figure 1-a) and belongs to the county of Ovar, an administrative region of Aveiro Portugal (Figure 1-b). Its coastal area and morphogenic dynamics is affected by maritime, wind and anthropic processes. The coastal area is defined by a very attractive and extensive sand beach suitable for touristic activities which in turn is increasing territorial vulnerabilities to the natural coastal dynamics. As a consequence, a fast urbanization took place which often covers primary dunes and directly affects the coastal processes.

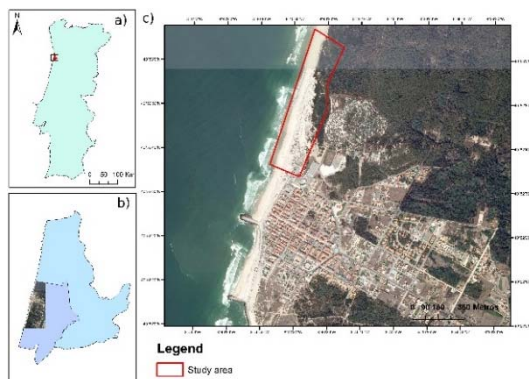


Figure 1: The study area: Furadouro's beach.

The (geo)morphology has been showing signs of several shoreline erosion processes, namely, those with oceanic and windy origins. These processes have

been reducing the sandy area of the beach while the ocean is advanced and gaining ground to the beach. Furthermore, with the occurrence of meteorological events, the action of such processes is accentuated. The urbanized areas of Furadouro already present several walled slopes on its south side, where residents aim at temporarily protect their properties. The recent construction of artificial bays at the north side of the beach will also increase the severity of these coastal processes generating more hazards and risks in this territory.

## 3 GEOSPATIAL DATA AND TECHNOLOGIES

### 3.1 Municipal Geospatial Data Archive

Two images of the historical United States Air Force (USAF) 1958 flight and 3 orthophotos series were used. These were obtained from the geospatial data archive of the municipality of Ovar. The radiometric quality (8 bits) of these digitalized UASF images are very poor and the camera calibration parameters are unknown. Therefore, it was impossible to use them in order to generate the DSM using a Structure from Motion and Multi-View Stereo (SfM-MV) approaches. Concerning the orthophotos they belong to the national coverage series published by the Portuguese Mapping Agency (Figure 2).

### 3.2 GNSS NRTK

The positioning survey method used for this study is based on NRTK approach. It uses the observations of GNSS acquired from the several Continuously Operating Reference Stations (CORS) network stations to model the error, at the rover, of the spatially correlated differences (the orbital errors and the ionospheric and tropospheric delays of the GNSS signal). The error is modelled assuming that these are constant for a given region. Merging the data coming from the multi-frequency GNSS receivers with the NRTK corrections available (national) both precision and accuracy are superior to the conventional RTK (using a single network station). Furthermore the NRTK solution offers a better coverage and reliability, more homogeneous accuracy and is faster when solving the ambiguities (Garrido et al., 2012). In this work the RENEP network with the geodetic system ETRS89, ETRF97 with year of reference 1995.4, was used. It broadcasts the differential corrections in real time in the format RTCM 3.1.,

which can be obtained via Internet with NTRIP (networked transport of RTCM via internet protocol). Network corrections using this approach allows the generation of positional accuracy and precision at a centimetre level (Aponte et al., 2009; Garrido et al., 2012; Pepe, 2018).



Figure 2: Two examples of geospatial data used in this study: the 2010 orthophoto and the 1958 image mosaic.

Ground Control Points (GCP) and cross profile survey tasks were performed with: i) two GNSS Geomax Zenith 10, equipped with triple frequency antennas (GPS, GLONASS, Galileo); ii) two wireless controllers GEOMAX PS339; iii) additional accessories such as tripods and targets. The planimetric coordinates (xy) of the geospatial data were referenced to the system ETRS89 PT/TM-06 (EPSG:3763) and the z coordinate to the geoid (orthometric altitude) using the numerical local geoid model GEODPT08.

### 3.3 Airborne LiDAR

LiDAR is commonly used in large scale shoreline mapping and change detection, due to its high geometrical accuracy, affordable costs and acquisition speed (Brock and Purkis, 2009). An airborne LiDAR system is basically composed of a

laser scanner, GNSS in differential mode and Inertial Measurement Unit (IMU). The typical data of a LiDAR survey is an irregular point cloud with three-dimensional coordinates where each point contains an ID (Petrie, 2011). This ID contains a given temporal mark and also the intensity of the received signal, the number of the return and quantity. The intensity of the reflected light is dependent on the surface characteristics, wave length of the laser and the incidence angle.

The LiDAR data used in this work is in a grid format and with spatial resolution of 1m. It was acquired with a LiDAR topographic LEICA ALS60 flying at a medium 1800m flight height between November, 17<sup>th</sup> and December, 7<sup>th</sup>, 2011.

### 3.4 UAS Photogrammetry

The low cost profile and versatility of UAV equipment combined with the advancements both in computer and photogrammetry were identified in literature (expand). The drone system is described in Table 1.

## 4 METHODOLOGY

The 2.5D digital representation of the coastline using high-resolution digital surface models, has been intensively employed in the topographical monitoring of coastal erosion (Mitasova et al., 2005). Such data can be further used in the study of several shoreline phenomena; for example, in coastal erosion simulations, flooding and monitoring coastal sediments (Mancini et al., 2013). The current paper, reveals the importance of the use of digital surface models obtained from UAV-images (dense image matching) and aerial LiDAR data. These were used to hand-made delineation of the coastline planimetric position for the years 2011 and 2015. The study of the coastal erosion has been taking advantage of high-resolution digital surface models (2.5D). Such information allows to perform simulations of coastal erosion, flooding phenomena and to monitor the balance of coastal sediments (Mancini et al., 2013).

The methodology adopted to determine shoreline change rates involves four main steps (Figure 3): 1) acquisition of the pertinent geospatial data for the period under evaluation; 2) manual digitalization of each shoreline and evaluation processes of the main error sources that affects the shoreline measurements in each category of geospatial data; 3) building of the shoreline time-series geodatabase and corresponding attribute data necessary for the GIS based DSAS

package; 4) computation of the shoreline change rates statistics.

Table 1: UAS specifications. G.C.S and D/W are the abbreviations for Ground Control Station and Dimensions/Weight, respectively.

Platform	
Type:	Quadcopter Tarot Iron Man 650
Engine Power:	4 T-Motor Navigator MN3110 470KV
Dim./weight:	95 cm / 1.5 kg (for all equipment)
Flight mode:	Manually based on wireless control
Endurance:	15 min (+ 3 min safety)
Digital camera	
Support:	Walkera G-2D Brusless gimbal
Camera model:	GoPro Hero4 Silver
→ Sensor type	CMOS - 1/2.3"
→ Pixel pitch [m]	1.54
→ Lens	Wide-angle lens
	<i>f/2.8 6-element aspherical glass</i>
→ Sensor window	Narrow FOV mode (focal 34.4 mm)
D/W:	41.0x59.0x29.6 mm / 84g
Flight control system	
Controller:	DJI Naza V2 (GPS)
G.C.S	Futaba 8J FHSS - FUTABA
	2-stick, 8-channel, S-FHSS, Built-in
	Dual Antenna Diversity
	Transmitting frequency: 2.4GHz band
FPV – Tx/Rx:	DJI Video Link 5.8Ghz 500mw
Monitor:	7" LCD
	Price: Approx. 1200 € (home assembled kit)

#### 4.1 Photogrammetric Workflow

The photogrammetric workflow used to produce the DSM and orthophoto from the set of UAV images

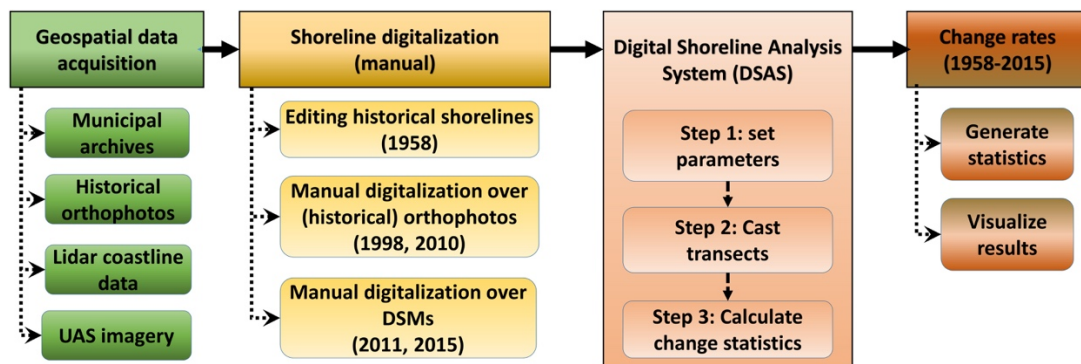


Figure 3: Workflow of the proposed methodology.

was performed in 3 main steps: 1) flight planning; 2) flight execution; 3) generation of both the DSM and orthophoto.

Regarding the step 1) several inputs were required. First, the ground pixel resolution (i.e. ground sampling resolution - GSD) must be defined. The flying height can then be determined for a given camera. Another issue is the image overlap (frontal 80% and lateral 60%), flying speed and corresponding shutter speed and distance between flying lines. Finally, the GCP must be well planned to allow a good Bundle Block Adjustment (BBA), since the direct georeferencing using the current drone was not possible (Rangel et al., 2018). Prior to the flying of the drone, targets were deployed in the area and their coordinates were acquired using a GNSS-NRTK method. Given that the drone can only be manually operated, a capture interval of five seconds image was introduced in the camera settings. The flying height was of 100m (GSD of 6 cm) and four flying lines were defined to be flown, parallel to the coastline. To generate the 3D model from the UAV images, Photoscan® was used. First we determined the tie points among all the 170 images. This allowed to calibrate the camera used in the study and to perform the relative and absolute orientation of the image block. This information was then used as input for the dense image matching performed in the last step, which gave us the final 3D point cloud. This final step for data acquisition process enabled the computation of the corresponding DSM and orthophoto.

#### 4.2 Accuracy Assessment of the DSM Derived from UAS Imagery

To assess the accuracy of the DSM derived from UAS imagery, we plot several terrain profiles which are perpendicular to the coast line. The DSM was then compared with two terrain cross profiles which were

recorded with GNSS-NRTK. For each planimetric position of the points that define the terrain profile we determined the height difference between the DSM and the ones obtained with the GNSS received in NRTK mode, henceforth referred as vertical residual. With these differences we determined the RMSE, mean and standard deviation.

### 4.3 Shoreline Proxy

In the literature, coastline and shoreline concepts may have different meanings (including in legal terms); however, in this study, these are used interchangeably being more conservative in spatial location than the physical interface of land and water, the latter being commonly used to define “shoreline”. Nevertheless, given the extreme shoreline dynamics, its mapping is usually based on an indicator/proxy. Considering that our goal is to monitor low-lying sandy beaches backed by dunes, the shoreline proxy used was the foredune toe. This proxy is described by either a slope break (break-line) and the seaward limit of vegetation, which are mainly covered by scattered vegetation (Figure 4). It is recognized as the morphological coastal feature less affected by short-term (tidal) and medium-term (seasonal) changes and was also used in previous studies (Ponte Lira et al., 2016), which mapped 92% and 95% of all the low-lying sandy beaches of mainland Portugal for the years 1958 and 2010, respectively.

In this work the two DSMs derived from LiDAR and UAS, were used as a base for the manual delineation of the planimetric position of the coastline for the years of 2011 and 2015 respectively. With the help of DSM hillshading techniques, it was possible to manually delineate the breaklines, corresponding to the position of the foredune toe.

### 4.4 Monitoring Shoreline Changes

Available for ArcGIS, the DSAS tool, allows the automation of processes that are required for the quantitative analysis of the evolution of a timeseries of shoreline data. Using equidistant terrain profiles delineated in GIS environment, these profiles were intersected with the shoreline of each epoch. These intersections were then used by several statistical methods to determine the increase/not-increase rates in the coastal erosion complex process.

In this work, we used the End Point Rate (EPR) the Linear Regression Rate (LRR) and the Weighted Linear Regression (WLR) methods. The EPR method determines the variation of the coastline dividing the distance of the coastal line movement by the time

going from the oldest to the most recent line (Thieler et al., 2009). The LRR method determines the retreat rate of the coastline using a simple linear regression, considering the variations present along each defined coastline. In this case, all the terrain profiles were considered in the statistical computations. However, these method tends to underestimate the rate of variation when compared with other statistical measures and its susceptible to extreme deviations (Thieler et al., 2009). Therefore, the WLR method tends to smooth the data by giving more emphasis or weight to the geospatial data for which the positional uncertainty is smaller. This weight ( $w$ ) is usually defined as a function of the variance in the uncertainty of the measurement ( $e$ ), that is:  $w = 1 / (e^2)$ , where  $e$  is the shoreline uncertainty value.

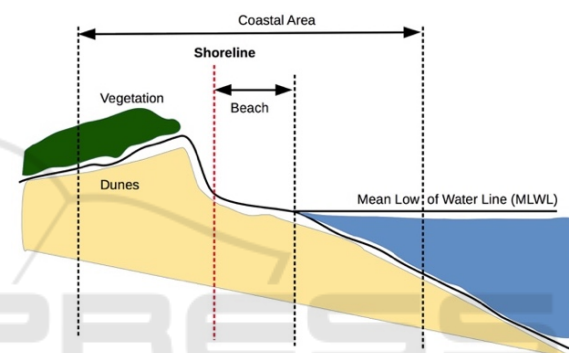


Figure 4: Shoreline proxy.

Moreover, it is possible to obtain some complementary measures, such as, the correlation coefficient, confidence interval and adjustment error.

### 4.5 Estimation of the Positional Uncertainty

Each geospatial mapping technology has its own sources of uncertainty, which in turn, affect the estimation of the shoreline change rate. These uncertainties are usually grouped in two categories (Fletcher et al., 2003): i) the measurement uncertainty, which is related to the characteristics of the data source technology and the operator-based measurement method; ii) the modeling (geometric representation of the shoreline) uncertainty which is related to all factors and phenomena that affect the spatial position of the real shoreline during a given year (e.g., stage of the tide, recent storms, seasonal state of the beach). In this study, the chosen shoreline proxy was affected by the following measurement uncertainties:

- Digitizing uncertainty ( $u_d$ ) – represents the uncer-

tainty produced by the operator due to some difficulties related to the visual interpretation of the shoreline. It was evaluated by digitizing several times the same shoreline on the same image,

- Resolution uncertainty ( $u_r$ ) – represents the smallest feature that is theoretically possible to identify on the geospatial product (image, ortho, DSM),
- Planimetric uncertainty ( $u_p$ ) – represents the horizontal accuracy that characterizes each specific source of data. For image data it was chosen the RMSE of the check points used in the registration process. For the orthophotos it was given by the RMSE of the aerotriangulation process and the published accuracy figures for each data set. For the case of surface data (LiDAR-based DSM and UAS-based DSM) the effect of the altimetric uncertainty ( $\sigma_z$ ) was also taken into account on the planimetric ( $\sigma_{zp}$ ) uncertainty by using the mean slope ( $\tan\alpha$ ) of the surface in the vicinity of the shoreline (Kraus, 1994):

$$\sigma_{zp} = \sigma_z / \tan\alpha \quad (1)$$

Assuming that these uncertainties are random and uncorrelated the total uncertainty quantified by calculating the square root of the sum of the squares of all uncertainties:

$$u_t = \sqrt{u_d^2 + u_r^2 + u_p^2} \quad (2)$$

Table 2 shows these uncertainties for each shoreline epoch. The uncertainty related with the digitalization of the shoreline ( $u_d$ ) was evaluated as the RMSE of the digitalization process carried out by 3 different operators.

## 5 RESULTS AND DISCUSSION

The proposed methodology for acquiring reliable shoreline information was implemented using the available UAS technology for the year 2015.

### 5.1 DSMs Derived from LiDAR and UAS

Figure 5 (a and b) shows, respectively, the orthophoto and DSM (0.10 m resolution) obtained by the UAS technology and used in the manual delineation of the coastline for the year 2015. Figure 5-c shows the DSM (1m resolution) obtained with LiDAR

technology and used in the manual delineation of the 2011 coastline.

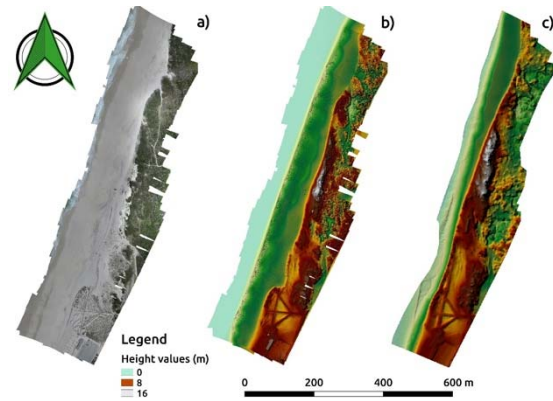


Figure 5: Orthophoto (a) and DSM (b) obtained from UAS imagery (2015); (c) DSM obtained from LiDAR (2011).

### 5.2 Accuracy Assessment of the DSM Derived from UAS Imagery

In Figure 6-a it can be seen the location of the three terrain profiles obtained by the GNSS-NRTK survey. Although these profiles are used for assessing the vertical accuracy of the DSM obtained by the UAS, these terrain profiles can also be used to observe the dynamics of Furadouro's beach for the period 2011-2015, when compared with the corresponding profiles interpolated from the DSM-LiDAR (Figure 6-b).

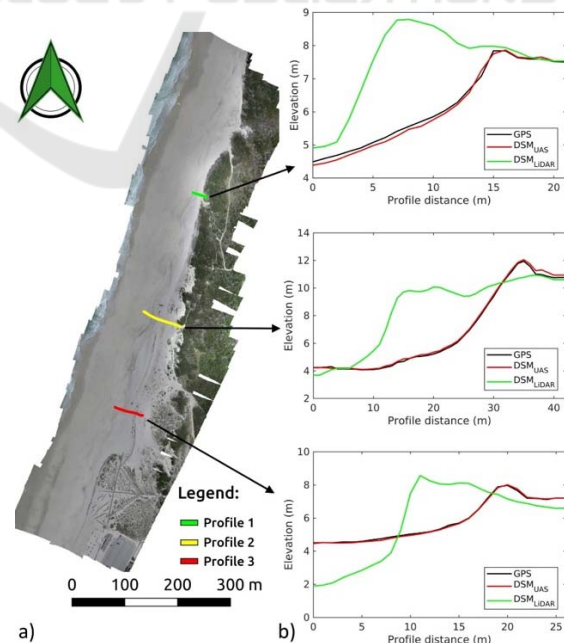


Figure 6: Location of the transversal profiles used to assess the vertical accuracy. b) Comparative analysis.

Table 2: Uncertainty (uncert.) measures.

Shoreline epoch	Acquisition technology	Digitalization mode	Spatial resolution	Digitizing uncert.	Resolution uncert.	Plan. uncert.	Total uncert.
1958	Film camera	Air photo	≈ 85 cm/pix	6 pix	2 pix	7.0 m	4.30 m
1998	Film camera	Ortho	≈ 50 cm/pix	4 pix	2 pix	2.2 m	2.30 m
2010	Digital camera	Ortho	50 cm/pix	2 pix	2 pix	0.7 m	0.80 m
2011	Airborne Lidar	DSM	≈ 1 pt/m2	75 cm	1.5 pix	0.5 m	0.50 m
2015	UAS imagery	Ortho+DSM	10 cm/pix	15 cm	1.5 pix	0.3 m	0.30 m

Comparing the two terrain profiles interpolated from the DSMs obtained from the UAS techniques, and the ones obtained directly from the GNSS-NRTK survey, we can compute some statistical measures for the vertical accuracy of the DSM. Table 3 illustrates some of the statistical measures for the positional accuracy (RMSE = 10 cm). It should be stressed that the mean varies from positive to negative between the profiles.

The normality of the distribution of the 92 residuals can be determined visually by two ways: generating the histogram and superimpose it with the normal distribution curve (Figure 7-a); or using a quantil-quantil (Q-Q) plot (Figure 7-b). Given that the curve of the graph Q-Q is close to the red line we can consider that we are facing a normal distribution of the residues, mean, RMSE and standard deviation of 10cm (1 GSD).

Table 3: Vertical accuracy indicators for UAS-DSM.

	N	RMSE (cm)	μ (cm)	σ (cm)
Profile 1	22	10	6	8
Profile 2	43	12	-9	8
Profile 3	27	5	3	5
Global	92	10	-2	10

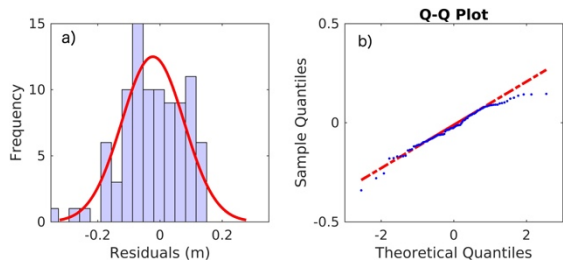


Figure 7: Normality testing for the profile residuals; a) Histogram with normal distribution curve; b) Q-Q plot.

### 5.3 Shoreline Changes

For this analysis we used the shorelines for the years 1958, 1998, 2010 and 2011, which were inserted into a geodatabase. A baseline from the shoreline

corresponding to the year 2015 was then drawn. This was performed by having a 15 m buffer around the 2015 shoreline.

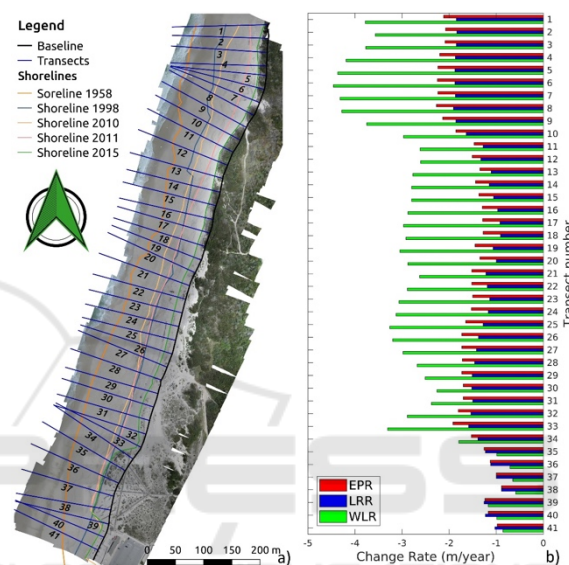


Figure 8: Evaluating the shoreline variation with DSAS: a) Location of the transects; b) Variation rates with three metrics (EPR, LRR e WLR).

Figure 8 shows the several retreat rates (negative values) of the shoreline for the 3 statistical measures (LRR, EPR and WLR). From the data we can observe that Furadouro has been through both coastal erosion and accretion. The latter corresponds to the temporal period 1998-2010 (profiles 15 to 37). It can also be observed the strong retreat process of the shoreline between 2010 and 2011, for example, profile 5 which presents a 46 m retreat process. From profile 8, and for the interval 1958-2015, a deeper and more evident retreat process -128 m can be observed (which is the maximum retreat value for the study area). Furthermore, the LRR has lower values in all of the profiles, exception being profiles 36 and 37. It needs to be noted that these profiles are located in an area already artificialized, namely with the construction of beach accesses and other recreational facilities. The highest mean value of the LRR corresponds to -1.9 m/year and the lowest -0.9 m/year. Concerning the EPR, this statistical measure presents the higher rates

of erosion, where it peaks at -2.3 m/year and minimum -0.89m/year. The mean retreat rate of the coastline for the 57 year interval considered in this study is of -1.5m/year. Some other figures can be stressed, for example, -1.4m/year for the LRR, -1.6m/year for the EPR and -2.7m/year for the WLR.

We can conclude that there was a generalized erosional continuous and complex process in the given time-frame. If we compare these results with previous studies, for example (Silva, 2012) and (Ponte Lira et al., 2016), we can conclude for the existence of some important discrepancies. Just to confirm this conclusion (Silva, 2012) reports the following retreat rates: -2.7 m/year from 1958 to 2010 and -4m/year for the period 2010/2012. In spite of the study area being larger than our study area, the time periods and the scale of analyses are also different. This and the reported work both present a coastal erosion process that surpasses 1.5 m per year.

## 6 CONCLUSIONS

Over the last decades, the Furadouro's beach has been suffering an increasingly severe shoreline retreat process. The DSAS tool was very effective in quantifying retreat rates, obtaining a mean value of -2.7 m / year (WLR) for the study area and for the 57 year time period: 1958 to 2015. In this work the DSM obtained by LiDAR aerial was undoubtedly an excellent starting point for the local monitoring of coastal erosion, since it allows for unambiguous definition of a temporal reference concerning the topographic position of the shoreline and the coastline surface and migrations process. In addition, it allows to integrate low-cost technologies (UASs) into local monitoring shoreline procedures. By allowing the generation of orthophotos and DSM, simultaneously, it is an added value in studies of coastal erosion at a local scale. Finally, it should be noted that the integration of several geospatial technologies in the topographic monitoring of the coastline also raises the need to standardize the concept of the coastline extracted from different geospatial data. As a final comment, these conclusions allow the authors to propose that increasing people awareness for the importance of hazards and risks mitigation and if we have in mind that Climate Changes are already producing substantive land and territorial changes, something must be done. It is our conviction that Geospatial technologies constitute a suite of interoperable tools that can support decision makers in order to implement a “culture of prevention”

instead of a “culture of reaction” as it has been argued by the UNESCO-ISDR (UNISDR, 2007).

## ACKNOWLEDGEMENTS

This work was partially supported by project grant UID/MULTI/00308/2019 and by the European Regional Development Fund through the COMPETE 2020 Programme, FCT - Portuguese Foundation for Science and Technology within the project PTDC/EAM-REM/30324/2017.

## REFERENCES

- Albuquerque, M., Espinoza, J., Teixeira, P., de Oliveira, A., Corrêa, I., Calliari, L., 2013. Erosion or Coastal Variability: An Evaluation of the DSAS and the Change Polygon Methods for the Determination of Erosive Processes on Sandy Beaches. *J. Coast. Res.* 165, 1710–1714. <https://doi.org/10.2112/SI65-289.1>
- Aponte, J., Xiaolin, M., Hill, C., Moore, T., Burbidge, M., Dodson, A., Meng, X., 2009. Quality assessment of a network-based RTK GPS service in the UK. *J. Appl. Geod.* 3, 25–34. <https://doi.org/10.1515/JAG.2009.003>
- Brock, J.C., Purkis, S.J., 2009. The Emerging Role of Lidar Remote Sensing in Coastal Research and Resource Management. *J. Coast. Res.* 10053, 1–5. <https://doi.org/10.2112/SI53-001.1>
- Cenci, L., Disperati, L., Persichillo, M.G., Oliveira, E.R., Alves, F.L., Phillips, M., 2017. Integrating remote sensing and GIS techniques for monitoring and modeling shoreline evolution to support coastal risk management. *GIScience Remote Sens.* 55, 1–21. <https://doi.org/10.1080/15481603.2017.1376370>
- Fletcher, C., Rooney, J., Barbee, M., Lim, S.C., Richmond, B., 2003. Mapping Shoreline Change Using Digital Orthophotogrammetry on Maui, Hawaii. *J. Coast. Res. Spec. Issue No. 38* 106–124.
- Garrido, M.S., Giménez, E., Armenteros, J.A., Lacy, M.C., Gil, A.J., 2012. Evaluation of NRTK positioning using the RENEP and RAP networks on the Southern border region of Portugal and Spain. *Acta Geod. Geophys. Hungarica* 47, 52–65. <https://doi.org/10.1556/AGeod.47.2012.1.4>
- Garrido, M.S., Giménez, E., Ramos, M.I., Gil, A.J., 2013. A high spatio-temporal methodology for monitoring dunes morphology based on precise GPS-NRTK profiles: Test-case of Dune of Mónsul on the south-east Spanish coastline. *Aeolian Res.* 8, 75–84. <https://doi.org/10.1016/j.aeolia.2012.10.011>
- Gonçalves, G.R., Pérez, J.A., Duarte, J., 2018. Accuracy and effectiveness of low cost UASs and open source photogrammetric software for foredunes mapping. *Int. J. Remote Sens.* 00, 1–19. <https://doi.org/10.1080/01431161.2018.1446568>

- Gonçalves, J.A., Henriques, R., 2015. UAV photogrammetry for topographic monitoring of coastal areas. *ISPRS J. Photogramm. Remote Sens.* 104, 101–111. <https://doi.org/10.1016/j.isprsjprs.2015.02.009>
- Hardin, E., Mitasova, H., Tateosian, L., Overton, M., 2014. GIS-based Analysis of Coastal Lidar Time-Series. <https://doi.org/10.1007/978-1-4939-1835-5>
- Kraus, K., 1994. Visualization of the quality of surfaces and their derivatives. *Photogramm. Eng. Remote Sensing* 60, 457–462.
- Mancini, F., Dubbini, M., Gattelli, M., Stecchi, F., Fabbri, S., Gabbianelli, G., 2013. Using unmanned aerial vehicles (UAV) for high-resolution reconstruction of topography: The structure from motion approach on coastal environments. *Remote Sens.* 5, 6880–6898. <https://doi.org/10.3390/rs5126880>
- Mitasova, H., Overton, M., Harmon, R.S., 2005. Geospatial analysis of a coastal sand dune field evolution: Jockey's Ridge, North Carolina. *Geomorphology* 72, 204–221. <https://doi.org/10.1016/j.geomorph.2005.06.001>
- Moore, L.J., 2000. Shoreline mapping techniques. *J. Coast. Res.* (ISSN 0749-0208) 16, 111–124. <https://doi.org/10.2112/03-0071.1>
- Pepe, M., 2018. CORS architecture and evaluation of positioning by low-cost GNSS receiver. *Geod. Cartogr.* 44, 36–44. <https://doi.org/10.3846/gac.2018.1255>
- Petrie, G., 2011. Airborne topographic laser scanners. *GEO Informatics* 34–44.
- Ponte Lira, C., Silva, A.N., Taborda, R., De Andrade, C.F., 2016. Coastline evolution of Portuguese low-lying sandy coast in the last 50 years: An integrated approach. *Earth Syst. Sci. Data* 8, 265–278. <https://doi.org/10.5194/essd-8-265-2016>
- Rangel, J.M.G., Gonçalves, G.R., Pérez, J.A., 2018. The impact of number and spatial distribution of GCPs on the positional accuracy of geospatial products derived from low-cost UASs. *Int. J. Remote Sens.* 00, 1–18. <https://doi.org/10.1080/01431161.2018.1515508>
- Silva, P.M.C., 2012. A tendência da linha de costa entre as praias de Maceda e S. Jacinto. *Universidade de Aveiro*.
- Sousa, W.R.N. de, Souto, M.V.S., Matos, S.S., Duarte, C.R., Salgueiro, A.R.G.N.L., Neto, C.A. da S., 2018. Creation of a coastal evolution prognostic model using shoreline historical data and techniques of digital image processing in a GIS environment for generating future scenarios. *Int. J. Remote Sens.* 00, 1–15. <https://doi.org/10.1080/01431161.2018.1455240>
- Thieler, E.R., Himmelstoss, E.A., Zichichi, J.L., Ergul, A., 2009. The Digital Shoreline Analysis System (DSAS) Version 4.0 - An ArcGIS extension for calculating shoreline change, Open-File Report. Reston.
- UNISDR, 2007. Towards a Culture of Prevention: Disaster Risk Reduction Begins at School [WWW Document]. URL [http://www.unisdr.org/files/761\\_education-good-practices.pdf](http://www.unisdr.org/files/761_education-good-practices.pdf) (accessed 3.12.19).